Optica Applicata, Vol. XXXIII, No. 2–3, 2003

Magnetooptical gratings with circular dots

JAROSLAV VLČEK[1], JAROMÍR PIŠTORA[1,2], DALIBOR CIPRIAN[1], TOMUO YAMAGUCHI[2], IVO VÁVRA[3]

[1]Department of Mathematics, Department of Physics, Technical University Ostrava, 17. listopadu 15, 708 33 Ostrava-Poruba, Czech Republic, e-mails: jaroslav.vlcek@vsb.cz, dalibor.ciprian@vsb.cz.

[2]Research Institute of Electronics, Shizuoka University, 3-5-1 Johoku, Hamamatsu 432, Japan, e-mails: rjpisto@ipc.shizuoka.ac.jp, rstyama@rie.shizuoka.ac.jp.

[3]Institute of Electrical Engineering, Slovak Academy of Sciences, Dúbravská cesta 9, Bratislava, Slovak Republic, e-mail: elekvavr@savba.sk.

The Kerr reflection is studied on various cases of binary magnetooptical grating with circular dots. The grating schemes proposed correspond to irregular grating preparation. Kerr rotation is calculated using theoretical model based on coupled wave method. The results obtained are compared with experimental data and discussed to find conditions of optimal coincidence.

Keywords: magnetooptical grating, Kerr effect, coupled wave method.

1. Introduction

Several of our recent experimental works and theoretical studies were concerned with an investigation of reflection properties (Kerr rotation) of two-dimensional magnetooptical (MO) gratings with the artificial anisotropy of permittivity induced by external magnetic field. The interest in magnetooptical grating multilayers corresponds to their wide applications to storage media, sensing devices or light modulators. Rich experimental results obtained at the Institute of Physics of the Technical University of Ostrava, Czech Republic, [1] required an appropriate theoretical tool for their consecutive analysis. We derived our own mathematical model [2] based on coupled wave method (CWM) implemented as the Fourier modal method (FMM).

As shown by the analysis based on atomic force microscopy (AFM), several of the analyzed gratings undergo certain shape irregularities in the course of preparation by ion milling. Also, residual impurities in the inter-dot area can be caused by "over -milling" into the substrate. In our study, the above factors were included in theoretical model to reach a better agreement between experiment and theory.

2. Experiments

Samples for measurements were prepared at the Institute of Electrical Engineering of Slovak Academy of Sciences. The gratings of an area of 1 mm^2 were etched by ion milling in the continuous 20 nm thick iron film sputtered on the Si/SiO_2 substrate, see Fig. 1. The resulting cylindrical dots rise the entire iron height and are ordered in bi-periodic grid. Geometrical parameters of any grating were established using AFM in a chosen domain, see Fig. 2 for example. In different gratings, the estimated dot radius r was in the range from 0.95 to 1.65 μm, the dimension Λ of square grating period varied from 4 to 4.3 μm. In order to represent this variability as simply as possible, we introduced the fill factor of the grating F, as the ratio "dot area/square period area", so that $F = \pi(r/\Lambda)^2$.

The measurements were concerned with specification of hysteresis loops of the Fe thin films and periodic gratings. The analyzed MO response allowed us to estimate

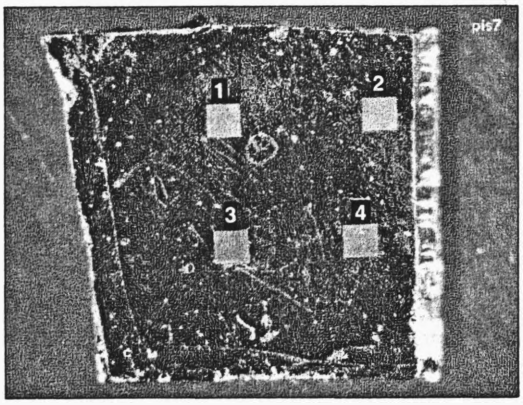

Fig. 1. Magnetooptical sample with 4 square gratings – a general view.

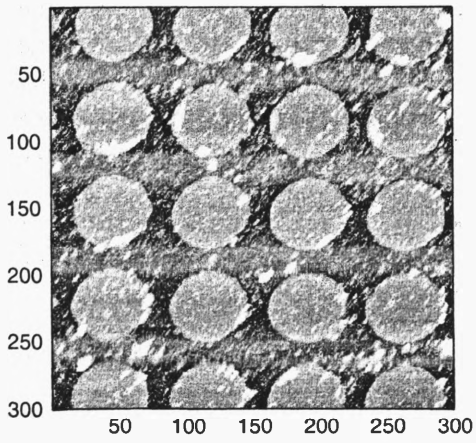

Fig. 2. Grating No. 4, the 17×17 μm AFM–frame (→ y-axis, ↑ x-axis).

Kerr rotation for various reflected diffraction orders. For details of the method and experimental setup used we refer to an earlier work of PIŠTORA *et al.* [1]. The Kerr rotation has been measured in the incidence plane for the incidence angle $\varphi = 45°$ at the wavelength $\lambda = 670$ nm. In numerical simulations the following material parameters were used: $n_{Fe} = 2.87 - 3.46i$, $Q_{Fe} = 0.0386 + 0.0034i$ (refractive index and the Voigt MO parameter of iron). All the media were supposed to be magnetically isotropic with permeability $\mu = 1$.

As the AFM analysis shows, the real grating geometry differs from expected ideal form, so that the shape irregularities of dots and grooves as well as impurities in the inter-dot area affect the results of experiments. In Figure 3, an example of the profile running through the centers of circular dots is shown. Unfortunately, using AFM we can estimate only the profile of grating surface, but not information about material properties.

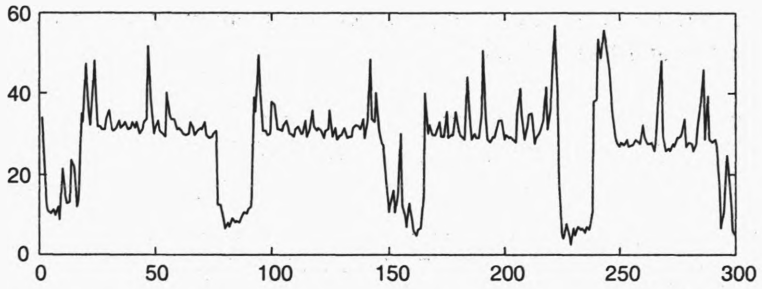

Fig. 3. Grating No. 4, vertical profile at row 150 in Fig. 2 (→ *y*-axis, ↑ *x*-axis).

Note that the vertical scale in Fig. 3 is in nanometers, however, the horizontal scale extending up to 17 μm is labelled in pixels. Therefore, this one is strongly compressed, which leads to seemingly large peaks and grooves.

Incident laser beam was linearly polarized in the incidence plane (*p*-polarization) or in orthogonal direction (*s*-polarization). Especially, the incidence plane was set to be parallel to external magnetic field **H** (the angle $\phi = 0$ in Fig. 5) that means a longitudinal geometry of the MO effect. Thereby, sufficiently high values of magnetic field strength were used to ensure a chosen geometry of Kerr effect in agreement with our formerly published experimental results in plain anisotropy of planar iron samples [3].

3. Basic theoretical model

The concepts prevailing in the modelling of periodical gratings favour the widely used coupled wave method frequently implemented as the FMM [4]–[6]. The mathematical model used here is based on the same principle with the following assumptions:

– the MO system under consideration is multilayered with one or more anisotropic layers separated by planar interfaces;

– the grating is created from anisotropic elements periodically patterned in isotropic medium; all the dots are of identical shape and they are fixed in the knots of bi-periodical rectangular grid;

– any layer is supposed to be homogeneous and isotropic in the direction perpendicular to interfaces, so that we speak about binary grating;

– admissible gratings satisfy the conditions $h << \Lambda_x$, $h << \Lambda_y$, where h is the layer thickness and Λ_x, Λ_y are the periods in main grid directions, respectively; this assumption ensures faithful application of FMM without the need of eventual convergence improvement [7].

To develop some efficient model of irregular gratings described in Sec. 2, we consider five forms of grating multilayer which correspond to the most important (but not all possible ones) tasks, see Fig. 4. In all the cases the modelled system contains only two kinds of layers: inhomogeneous domain with periodic space modulation or a homogeneous layer (sub- or superstrate, remaining Fe film by partial etching). The basic configuration (Fig. 4**a**) has been studied in [2] especially from the point of view a relation between fill factor and Kerr reflection.

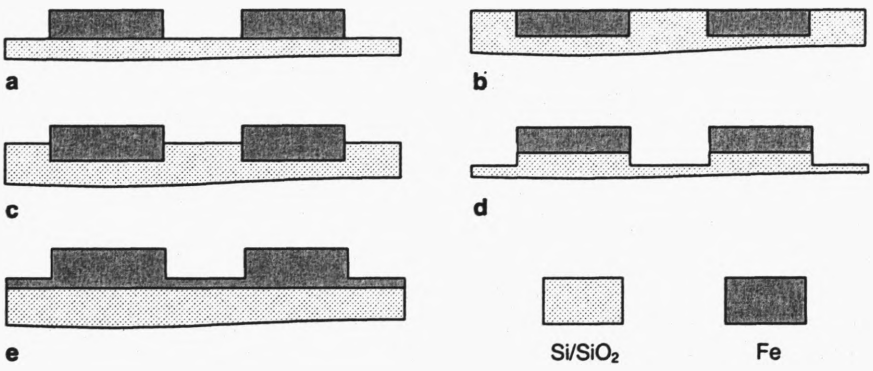

Fig. 4. Typology of binary gratings: original model (**a**), fully (**b**), and partially filled (**c**) grating; over -etched (**d**), and partially etched (**e**) grating.

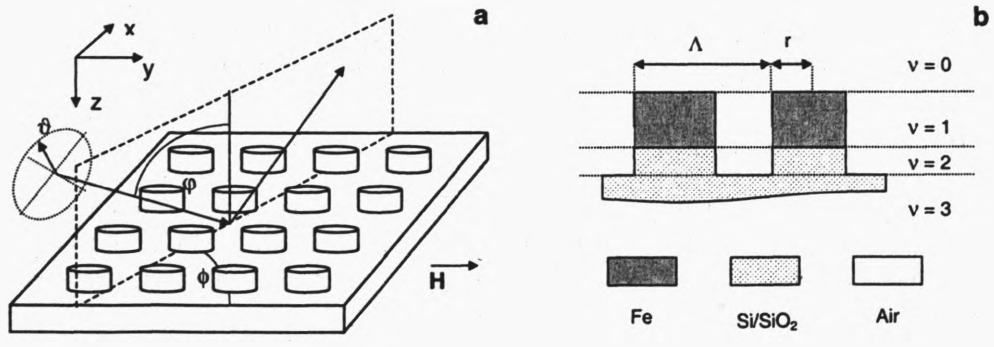

Fig. 5. Coordinate system and incident wave (**a**), and the scheme of a multilayer (**b**).

The coordinate system is introduced as in Fig. 5. Generally, the layers of the grating structure are indexed toward growing z coordinate and their thickness is denoted by $h(\nu)$, $\nu = 1,\ldots, K$. The multilayer is sandwiched between two semi-infinite isotropic regions, the substrate ($\nu = K + 1$ for $z > h^{(1)} + \ldots + h^{(K)}$) and the superstrate ($\nu = 0$ for $z < 0$).

Incident monochromatic plane wave with free space wavelength λ propagates in the homogeneous isotropic superstrate with refractive index $n^{(0)}$. The wave vector forms an angle φ relative to z-axis and these two directions define the incidence plane. Its deviation from the y-axis is denoted by angle ϕ. Generally, the incident polarized state is elliptical and defined by the angle ϑ between unit-amplitude electrical field vector and the incidence plane.

A representation of field components and material functions by two-fold Fourier expansion is the basic principle of the FMM. Introducing dimensionless space coordinates $(x_1, x_2, x_3) = k_0(x, y, z)$, $k_0 = 2\pi/\lambda$, the components of field vectors can be obtained in the form ($j = 1, 2, 3$)

$$E_j^{(\nu)}(x_1, x_2, x_3) = \sum_m \sum_n \sum_q u_q^{(\nu)} e_{jmnq}^{(\nu)} \exp\{-i(\alpha_m x_1 + \beta_n x_2 + \gamma_q^{(\nu)} x_3)\}, \tag{1}$$

$$H_j^{(\nu)}(x_1, x_2, x_3) = \sum_m \sum_n \sum_q u_q^{(\nu)} h_{jmnq}^{(\nu)} \exp\{-i(\alpha_m x_1 + \beta_n x_2 + \gamma_q^{(\nu)} x_3)\} \tag{2}$$

where $\alpha_m = n^{(0)} \sin\phi \sin\varphi + \lambda m/\Lambda_x$, $\beta_n = n^{(0)} \cos\phi \sin\varphi + \lambda n/\Lambda_y$. Since in real computations only the finite number of harmonic components is used, we truncate both the index sets by appropriate chosen values M, N, so that $-M \le m \le M$, and $-N \le n \le N$.

In any layer the boundary value problem for the Maxwell partial differential equations is reformulated to an algebraic eigenvalue problem. Its solution leads to propagation constants $\gamma_n^{(\nu)}$ and polarisation states at single diffraction orders, represented by eigenvectors $\mathbf{e}_{jq}^{(\nu)}$, $\mathbf{h}_{jq}^{(\nu)}$ of Fourier coefficients with dimension $d = (2M + 1) \times (2N + 1)$ regarding finite truncation of mode orders. Note that for an isotropic homogeneous layer the eigenvalues and eigenvectors can be exactly derived. For futher details of the CWM model used refer to paper [2].

The wave coupling in the multilayer follows from application of boundary conditions on layer interfaces to tangential field components in the form:

$$E_j^{(\nu)} = E_j^{(\nu+1)}, \quad H_j^{(\nu)} = H_j^{(\nu+1)}, \quad j = 1, 2. \tag{3}$$

Using Fourier representation of field components we obtain a 4D algebraic system for vectors $\mathbf{u}^{(\nu)}$ of amplitude coefficients in the superstrate (incident and reflected fields) and substrate (transmitted field):

$$\mathbf{u}^{(0)} = \mathbf{M} \cdot \mathbf{u}^{(K+1)}, \quad \mathbf{M} = (\mathbf{D}^{(0)})^{-1} \cdot \prod_{\nu=1}^{K} \mathbf{S}^{(\nu)} \cdot \mathbf{D}^{(K+1)} \tag{4}$$

where any layer of the thickness $h^{(\nu)}$ contributes to the matrix $\mathbf{M}$ by the term $\mathbf{S}^{(\nu)} = \mathbf{D}^{(\nu)} \cdot \mathbf{P}^{(\nu)} \cdot (\mathbf{D}^{(\nu)})^{-1}$. The matrix $\mathbf{D}^{(\nu)}$ is composed of 4D column vectors of the form $(\mathbf{e}_1\ \mathbf{h}_2\ \mathbf{e}_2\ \mathbf{h}_1)^{\mathrm{T}}$

$$\mathbf{D}^{(\nu)} = \begin{bmatrix} [\mathbf{e}_{1q}]_s^+ & [\mathbf{e}_{1q}]_p^+ & [\mathbf{e}_{1q}]_s^- & [\mathbf{e}_{1q}]_p^- \\ [\mathbf{h}_{2q}]_s^+ & [\mathbf{h}_{2q}]_p^+ & [\mathbf{h}_{2q}]_s^- & [\mathbf{h}_{2q}]_p^- \\ [\mathbf{e}_{2q}]_s^+ & [\mathbf{e}_{2q}]_p^+ & [\mathbf{e}_{2q}]_s^- & [\mathbf{e}_{2q}]_p^- \\ [\mathbf{h}_{1q}]_s^+ & [\mathbf{h}_{1q}]_p^+ & [\mathbf{h}_{1q}]_s^- & [\mathbf{h}_{1q}]_p^- \end{bmatrix} \tag{5}$$

(the layer index ν is omitted). The structure of matrix $\mathbf{D}^{(\nu)}$ allows dividing the field into forward (+) and backward (–) modes, which are further distinguished regarding both the basic *s*- and *p*-polarizations. Diagonal elements of the matrix $\mathbf{P}^{(\nu)} = \mathrm{diag}\{\exp(ik_0\gamma_q^{(\nu)}h^{(\nu)})\}$ express the propagation of q-th mode through the ν-th layer. Supposing that no wave propagates from the substrate, we solve Eq. (4) for amplitude coefficients in two cases,

$$\begin{bmatrix} \mathbf{u}_s^{(0)+} \\ \mathbf{o} \\ \mathbf{u}_{ss}^{(0)-} \\ \mathbf{u}_{sp}^{(0)-} \end{bmatrix} = \mathbf{M} \cdot \begin{bmatrix} \mathbf{u}_{ss}^{(K+1)+} \\ \mathbf{u}_{sp}^{(K+1)+} \\ \mathbf{o} \\ \mathbf{o} \end{bmatrix} \quad \text{or} \quad \begin{bmatrix} \mathbf{o} \\ \mathbf{u}_p^{(0)+} \\ \mathbf{u}_{ps}^{(0)-} \\ \mathbf{u}_{pp}^{(0)-} \end{bmatrix} = \mathbf{M} \cdot \begin{bmatrix} \mathbf{u}_{ps}^{(K+1)+} \\ \mathbf{u}_{pp}^{(K+1)+} \\ \mathbf{o} \\ \mathbf{o} \end{bmatrix}, \tag{6}$$

correspondingly to a given polarization state of unit-amplitude incident wave, *i.e.*, for

$$\mathbf{u}_s^{(0)+} = \delta_{0m}\delta_{0n} = \mathbf{u}_p^{(0)+}, \qquad m = -M, \ldots, M, \qquad n = -N, \ldots, N.$$

Magnetooptical activity of a grating is expressed in the reflected field by Kerr rotation and ellipticity. Denoting

$$X_q = \frac{u_{sp,q}^{(0)-}}{u_{ss,q}^{(0)-}} \quad \text{or} \quad X_q = \frac{u_{ps,q}^{(0)-}}{u_{pp,q}^{(0)-}}$$

regarding incident polarization (first subscript of amplitude coefficients), we can calculate the rotation θ by the formula [8]

$$\theta = \frac{1}{2}\arctan\left(\frac{2\mathrm{Re}(X_q)}{1-|X_q|^2}\right). \tag{7}$$

4. Numerical results

The algorithm derived was implemented in the Matlab6.0 code and operated on standard personal computer with the 733-MHz Pentium III® processor and 128-Mbyte memory. The input data correspond to experimental arrangement described, which means longitudinal configuration of MO effect, incidence angle 45° and square grating period $\Lambda_x = \Lambda_y = \Lambda$. The latter leads to equal truncation orders $M = N$, which implies global dimension of eigenvalue problem $4(2M + 1)^2$. For instance, this means for a basic model with one inhomogeneous layer 1156 modes and 12.9 minutes of computational time for truncation order $M = 8$. An error less than 10^{-7} was obtained in the case of ideal media for both polarizations.

Two gratings with different geometrical parameters given by fill factor F are presented in our comparative study, for which the structural models shown in Fig. 4 are considered. Tables 1 and 2 summarize measured and calculated values of the Kerr rotation θ in mrad. These results correspond to the modes in the incidence plane $x = 0$ at the lowest diffraction orders, for which $k = 0$ and $l = -1, 0, 1$. Longitudinal geometry

T a b l e 1. Grating No. 1: Kerr rotation θ in mrad for various grating models.

Grating No. 1 $F = 0.170$		Orders for *s*-polarization			Orders for *p*-polarization		
		–1	0	1	–1	0	1
Experiment		0.73	0.37	1.11	1.09	–0.16	1.23
Basic model		1.61	0.49	2.55	0.94	–0.99	1.02
Partially filled grating up to	5 nm	1.60	0.41	2.51	0.90	–0.93	0.99
	10 nm	1.57	0.41	2.47	0.87	–0.82	0.97
Fully filled grating		1.45	0.40	2.33	0.82	–0.57	0.91
Over-etched grating by	2 nm	1.61	0.41	2.55	0.93	–0.98	1.01
	4 nm	1.61	0.41	2.55	0.93	–0.97	1.01
Imperfectly etched grating		1.61	0.59	2.88	1.10	–2.39	1.04

T a b l e 2. Grating No. 2: Kerr rotation θ in mrad for various grating models except an over-etching.

Grating No. 2 $F = 0.475$		Orders for *s*-polarization			Orders for *p*-polarization		
		-1	0	1	-1	0	1
Experiment		0.69	0.81	1.19	1.03	-0.07	1.32
Basic model		1.33	0.79	2.13	0.77	3.66	0.97
Partially filled grating up to	5 nm	1.33	0.78	2.10	0.75	3.98	0.96
	10 nm	1.32	0.77	2.07	0.74	4.03	0.84
Fully filled grating		1.25	0.74	1.98	0.71	3.45	0.79
Imperfectly etched grating		1.29	0.84	2.35	0.87	2.23	0.84

of MO effect mentioned above implies very small amplitude coefficients at zero diffraction order for *p*-polarized incident beam. This may be the reason of the difference between experimental and theoretical values, as well as of several data shifts (see the last row in Tab. 1).

The results of numerical simulation presented in Tab. 1 permit us to draw several conclusions related to chosen grating features. At first, an over-etching into the substrate by a few nanometers has rather no influence on the Kerr rotation. Similarly, an imperfect etching is of little importance except the *p*-polarized mode at zero diffraction order due to the above mentioned data inaccuracy. In particular, we chose in this model the etching depth 18 nm by the entire height of iron layer 20 nm.

A fully filled or partially filled grating contains badly determinable material within inter-dot grooves. By mathematical simulation we suppose that refractive indexes of the filler and substrate are equal. As filler height increases up to the fully filled case, theoretical values of Kerr rotation by *s*-polarized input approach experimental data. An interpretation for *p*-polarized beam is not unique yet, because the non-zero diffraction orders show opposite tendency.

A change of the grating geometry brings about the same trends, as can be seen in Tab. 2. Here the data are measured and calculated for three times greater fill factor F. It follows from the two tables that increased ratio of ferromagnetic component in a geometrically modulated layer (*i.e.*, by growing fill factor) leads to decreasing dependence of MO effect on geometrical irregularities described. Note that the reason of asymmetry for Kerr rotation angle between diffraction orders –1 and +1 is the difference of their tangential field components.

5. Conclusions

The results obtained confirm the fact that small over-etching into the substrate or incomplete etching play the minor role in Kerr rotation, when their size is much less than dot height. On the other hand, a subsequent fill of the inter-dot area with another material (remainder of protection cover or of etched medium) seems to be more important. To solve this problem, the material properties of the filler should be specified more correctly.

References

[1] PIŠTORA J., BÁRTA O, VLČEK J., CIPRIAN D., HRABOVSKÝ D., VÁVRA I., SMATKO V., KOVÁČOVÁ E., POSTAVA K., KOPŘIVA I., *2D Optical Gratings with Magnetic Ordering*, Proceedings of the 8th International Symposium on Microwave and Optical Technology, [Ed.] K. Wu, A.B. Kouki, B.S. Rawat, Polytechnic International Press, Montreal, Canada 2001, pp. 437–441.

[2] VLČEK J., PIŠTORA J., CIPRIAN D., YAMAGUCHI T., POSTAVA K., Trans. Magn. Soc. Jap. **2** (2002), 179.

[3] POSTAVA K., BOBO J.F., ORTEGA M.D., RAQUET B., JAFFRES H., SNOECK E., GOIRAN M., FERT A.R., REDOULES J.P., PIŠTORA J., OUSSET J.C., J. Magn. Magn. Mat. **163** (1996), 8.

[4] NOPONEN E., TURUNEN J., J. Opt. Soc. Am. A **11** (1994), 2494.
[5] LI L., J. Mod. Opt. **45** (1998), 1313.
[6] VIŠŇOVSKÝ Š., YASUMOTO K., Czech J. Phys. **51** (2001), 229.
[7] POPOV E., NEVIÈRE M., J. Opt. Soc. Am. A **17** (2000), 1773.
[8] AZZAM R.M.A., BASHARA N.M., *Ellipsometry and Polarized Light*, North-Holland Publ. Comp., Amsterdam 1977.

Received November 15, 2002
in revised form December 11, 2002